ACS APPLIED MATERIALS & INTERFACES

Research Article

www.acsami.org

Nanoclay Gelation Approach toward Improved Dye-Sensitized Solar Cell Efficiencies: An Investigation of Charge Transport and Shift in the TiO_2 Conduction Band

Xiu Wang,[†,○] Sneha A. Kulkarni,[‡,○] Bruno Ieiri Ito,[§] Sudip K. Batabyal,[‡] Kazuteru Nonomura,[‡,▽] Chee Cheong Wong,[†] Michael Grätzel,[▽,⊥] Subodh G. Mhaisalkar,*[,†,‡,▽] and Satoshi Uchida*[,§]

[†]School of Materials Science & Engineering, Nanyang Technological University, Block N4.1 Nanyang Avenue, Singapore 639798

[‡]Energy Research Institute @ NTU (ERI@N), Nanyang Technological University, Research Techno Plaza, RTP/XF-05 50 Nanyang Drive, Singapore 637553

[§]Department of Applied Chemistry, Graduate School of Engineering, The University of Tokyo, 3-8-1 Komaba, Meguro-ku, Tokyo 153-8902, Japan

[▽]Center for Nanostructured Photosystems (CNPS), Nanyang Technological University, Research Techno Plaza, RTP/XF-05 50 Nanyang Drive, Singapore 637553

[⊥]Laboratory of Photonics and Interfaces, École Polytechnique Fédérale de Lausanne, CH-1015 Lausanne, Switzerland

Supporting Information

ABSTRACT: Nanoclay minerals play a promising role as additives in the liquid electrolyte to form a gel electrolyte for quasi-solid-state dye-sensitized solar cells, because of the high chemical stability, unique swelling capability, ion exchange capacity, and rheological properties of nanoclays. Here, we report the improved performance of a quasi-solid-state gel electrolyte that is made from a liquid electrolyte and synthetic nitrate-hydrotalcite nanoclay. Charge transport mechanisms in the gel electrolyte and nanoclay interactions with TiO_2/electrolyte interface are discussed in detail. The electrochemical analysis reveals that the charge transport is solely based on physical diffusion at the ratio of [PMII]:[I_2] = 10:1 (where PMII is 1-propyl-3-methylimidazolium iodide). The calculated physical diffusion coefficient shows that the diffusion of redox ions is not affected much by the viscosity of nanoclay gel. The addition of nitrate-hydrotalcite clay in the electrolyte has the effect of buffering the protonation process at the TiO_2/electrolyte interface, resulting in an upward shift in the conduction band and a boost in open-circuit voltage (V_{OC}). Higher V_{OC} values with undiminished photocurrent is achieved with nitrate-hydrotalcite nanoclay gel electrolyte for organic as well as for inorganic dye (D35 and N719) systems. The efficiency for hydrotalcite clay gel electrolyte solar cells is increased by 10%, compared to that of the liquid electrolyte. The power conversion efficiency can reach 10.1% under 0.25 sun and 9.6% under full sun. This study demonstrates that nitrate-hydrotalcite nanoclay in the electrolyte not only solidifies the liquid electrolyte to prevent solvent leakage, but also facilitates the improvement in cell efficiency.

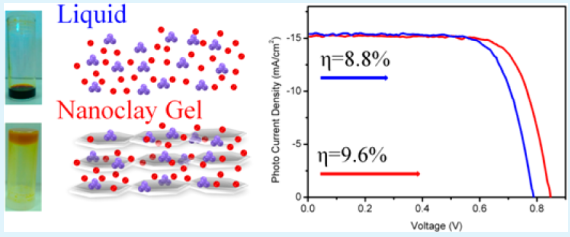

KEYWORDS: *quasi-solid state, anionic nanoclay, hydrotalcite, gel electrolyte, dye-sensitized solar cells (DSCs)*

INTRODUCTION

Dye-sensitized solar cells (DSCs) have aroused intense interest because of their high energy conversion efficiency, simplicity, low cost, and environmentally friendly fabrication method.[1,2] Previously, much effort has been exerted toward enhancing the device efficiency through optimizing individual cell components.[3−7] So far, single cell efficiency of 12.3% and module efficiency of 9.9% have been reported, which makes this technology competitive.[8,9] However, for liquid DSCs, several critical technical problems limit long-term performance and practical use, in particular, the leakage or evaporation of volatile solvent.[10−14] Consequently, much attention has been focused on improving the liquid electrolytes or substituting liquid electrolytes with solid-state or quasi-solid-state electrolytes.[15,16] Some efforts have been made to fabricate solid-state DSCs, which did not require hermetic sealing. However, lower solar to electric power conversion efficiency (PCE) was observed, compared to that of liquid DSCs, which may be due to low hole conductivity, poor pore-filling ability, and/or poor electrode contact.[12,17,18] Recently, quasi-solid-state electrolytes have emerged to be very good candidates to be applied in DSCs, because of their twin attributes: the cohesive property of a solid and the diffusive capacity of a liquid.[19] One particular approach is to form the quasi-solid-state electrolyte, using inorganic nanoparticles as additives in various ionic liquids in order to increase the viscosity as well as electrode−electrolyte interfacial

Received: November 1, 2012
Accepted: December 19, 2012
Published: December 19, 2012

contact.[20,21] For example, a composite ionic liquid electrolyte formed by mixing silica nanoparticles into 1-propyl-3-methylimidazolium iodide (PMII) has shown a high conversion efficiency of 7.0%.[22] Comparing to liquid devices, the advancement of quasi-solid-state DSCs is still a gradual process.

Recently, clay minerals have attracted attention as an additive in electrolytes, because of their high chemical stability, unique swelling ability, ion exchange capacity, abundance in nature, and rheological properties.[23,24] Tu et al. demonstrated that polymer-gelled DSCs incorporated with montmorillonite clay showed enhancement in efficiency due to a decrease in electrolyte-contact resistance.[25] Later, Park et al. deduced the unexpected benefits of clay gel electrolyte, because of the light scattering capability of laponite clay.[26] Furthermore, Tsui and co-workers attempted to use modified montmorillonite with long alkyl chain to form clay type nanocomposite and proposed that the space between the clay can offer a wider transfer path for iodide/triiodide.[27] Inoue et al. showed high cell performance of 10.3% for clay gelled electrolyte, equivalent in performance to liquid electrolyte cells.[28]

Even though nanoclay has proven to be one of the promising additives to gel the liquid electrolyte, efficiency enhancement of the top performing cells is still in progress.[26,28] As discussed previously, besides solidifying the electrolyte, the role played by nanoclay additives on the photoelectrochemical performance of the device has not yet been elucidated in detail. According to earlier studies in photochemistry and photocatalysis, smectite clay hinders the diffusion of anions, while cations incorporated in the clay films can induce electrocatalytic effects.[29,30] Apparently, much study needs to be carried out to reveal the effect of clay in photovoltaic devices, viz, the clay interaction with the electrolyte of DSCs, especially in its gel form, and correlation of interaction with charge transport mechanism in device, etc. The nanoclays used in previous studies were mainly of smectite/montmorillonite type, which belong to the family of cationic clays (hydroxides layers with negative charge). Since the active redox species (triiodide/iodide) present in the current DSC systems are anions, anionic nanoclay (the net positive charge of octahedral layers is balanced by an equal negative charge from the interlayer anions[31]) additives in the gel electrolyte may be expected to have better ability, in terms of interaction/intercalation with the electrolyte.

In the current work, we report the synthesis of a quasi-solid-state gel electrolyte that consists of a liquid electrolyte and synthetic nitrate–hydrotalcite nanoclay that solidifies the liquid electrolyte and improves the PCE. Cyclic voltammetry provides the information on the charge transport in gel electrolyte, whereas electrochemical impedance spectroscopy gives a broad view of resistance and capacitance of each component. The obtained results are combined in a coherent picture in order to identify the effect of nitrate–hydrotalcite nanoclay in a gel electrolyte system.

RESULTS AND DISCUSSION

Nitrate-Hydrotalcite Gel in Dye-Sensitized Solar Cells (DSCs). The photocurrent density–voltage (J–V) characteristics of the DSCs with liquid and 10 wt % nanoclay gel electrolyte under one sun illumination are listed in Table 1. Better device performance was observed using acetonitrile (AN) rather than methoxypropionitrile (MPN) as the solvent to prepare the electrolyte. In fact, the higher device efficiencies for an AN-based electrolyte are mainly due to the better fill factor, which reflects the resistance level in the device. It could be due to the higher ionic conductivity of AN over MPN.[32] Even so, irrespective of the solvent, a higher PCE was achieved for nitrate-hydrotalcite nanoclay gel devices: the short-circuit current density (J_{SC}) and fill factor (FF) values were comparable to those of liquid versions, along with significant enhancement in open-circuit voltage (V_{OC}).

Table 1. Comparison of the Photovoltaic Characteristics Based on Liquid and Gel Electrolyte in Different Solvents (AN and MPN) under One Sun Illumination

solar cell[a]	PCE (%)	J_{SC} (mA/cm^2)	V_{OC} (mV)	FF	ΔPCE[b] (%)
L-MPN	7.0	15.2	741	0.62	
G-MPN	7.9	15.4	843	0.61	13
L-AN	8.8	15.3	786	0.73	
G-AN	9.6	15.1	846	0.75	9

[a]L-MPN and G-MPN refer to, respectively, liquid and nanoclay gel electrolyte prepared using methoxypropionitrile; L-AN and G-AN refer to liquid and nanoclay gel electrolyte in acetonitrile. Data are obtained with photoanode 5 + 2 layers. [b]Calculated using ΔPCE = $(PCE_G - PCE_L)/PCE_L$.

Charge Transport in Nanoclay Gel. The observed J_{SC} for both liquid and gel electrolyte devices are comparable; moreover, the linear increase of J_{SC} with light intensity clearly indicates that the reaction rate of redox ions to dye is fast enough for regeneration (Figure 1). It suggests that viscosity of nanoclay gel does not have much of an effect on charge transport in the electrolyte. Unlike in some other types of polymer/gel system, cells often perform better under low-intensity illumination, because of the diffusion-limited J_{SC} that is observed under high-intensity illumination.[33,34] It has been proposed that, in nanocomposite gelled electrolytes typically in ionic liquids, besides the physical diffusion (in most liquid systems), another type of charge transport mechanism (called Grotthus type or exchange-reaction process, $I^- + I_3^- \rightarrow I_3^- + I^-$) may also assist the current flow.[35−37] In such cases, rapid charge transfer is enabled, even in a viscous medium, since physical species transfer is not necessary for charge transport. It may be due to the adsorption of redox ions on the particle surface forming a dense and oriented redox region by electrostatic interaction, which may act as a rapid charge transport path with an exchange reaction.[20,38,39] It was also illustrated that the clay significantly affects the diffusion of the ions if applied to electrodes.[40−42] Taking into account these arguments for nanoclay gel system, it is suggested that

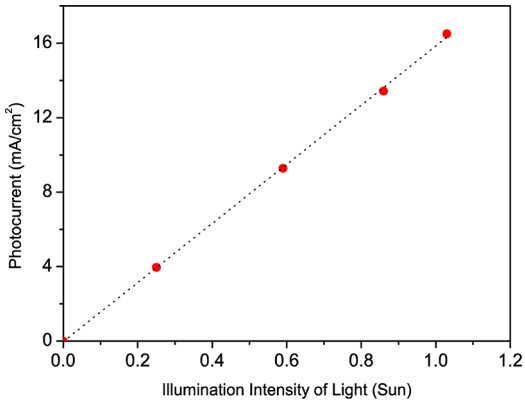

Figure 1. Photocurrent of G-AN under various illumination conditions (0.25, 0.59, 0.86, and 1.03 sun).

dx.doi.org/10.1021/am3025454 | ACS Appl. Mater. Interfaces 2013, 5, 444−450

fundamental studies, such as the charge transport mechanism and equilibrium potentials of redox couple in the gel system, have not been revealed yet, although the understanding of such characteristics is crucial for DSC applications.

Steady-state cyclic voltammetric analysis was carried out in order to understand the charge transport mechanism in the nitrate-hydrotalcite gel electrolyte system. The limited current (I_{lim}) in cyclic voltammograms, corresponding to the reaction $I_3^- + 2e^- = 3I^-$, is given by[35]

$$I_{lim} = 8FDrc \quad (1)$$

where D is the diffusion coefficient of redox species, r the microdisk electrode radius, and c the total concentration of the redox species ($^1/_3[I^-] + [I_3^-]$). If physical diffusion and the Grotthus mechanism are conjugated, then

$$D = D_{phys} + D_{ex} \quad (2)$$

$$= D_{phys} + \left(\frac{1}{6}\right)k_{ex}\delta^2 c \quad (3)$$

where D_{phys} and D_{ex} are the respective coefficients based on simple physical diffusion and Grotthus/exchange reaction, k_{ex} is the exchange reaction rate constant, and δ is the center-to-center intersite distance at the exchange reaction. Substituting eq 3 into eq 1 gives

$$I_{lim} = 8Fr\left[D_{phys}c + \left(\frac{1}{6}\right)k_{ex}\delta^2 c^2\right] \quad (4)$$

Consequently, according to eq 4,[35] pure physical diffusion predicts a linear relationship of limiting current as a function of total concentration of redox species, while pure exchange predicts quadratic behavior. As shown in Figure 2, at a fixed ratio of [PMII]:[I_2] = 10:1, limiting current with concentration of redox species exhibits a linear relationship with correlation coefficients of $R^2 > 0.985$. It clearly indicates that the charge transportation in nitrate-hydrotalcite gel electrolyte is conducted solely by physical diffusion at a ratio of [PMII]:[I_2] = 10:1. Furthermore, the calculated physical diffusion coefficient of I_3^- shows independence with concentration variation, which also supports typical physical diffusion behavior. Although the gel electrolyte is viscous in nature, redox ions can still diffuse smoothly, because of the unique properties of nanoclay forming three-dimensional (3-D) networks and providing channels for diffusion. Although calculated DI_3^- in nanoclay gel is slightly smaller than that in liquid, it does not result in a major deficiency in photocurrent collection.

The presence of iodide ions[43,44] in the clay powder extracted from the nanoclay gel electrolyte clearly reveals that, besides diffusing through the network structure, the iodide ions are also accommodated by the nitrate-hydrotalcite nanoclay particles (see Figure 3a). In addition, the presence of iodide was not found in a reference clay sample that was extracted from the electrolyte under the same procedure (details given in the Supporting Information (SI)). Thus, the probability of the

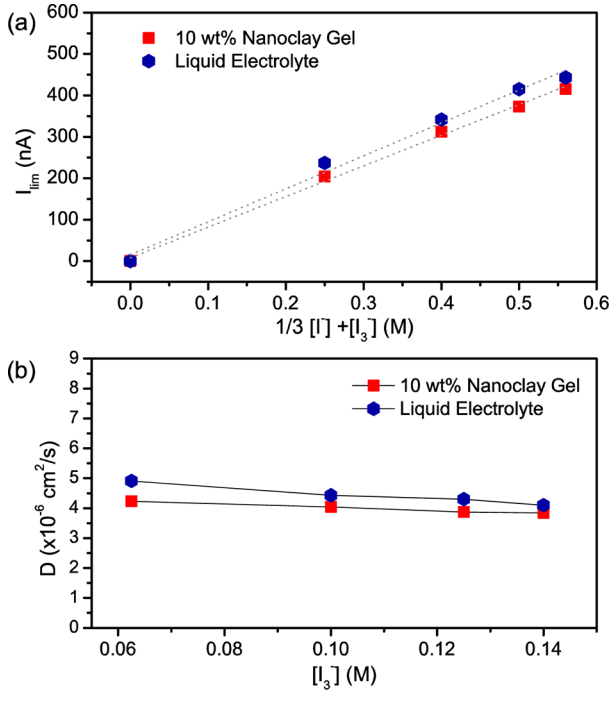

Figure 2. (a) Limiting currents for reaction of $I_3^- + 2e^- = 3I^-$, as a function of concentration ($^1/_3[I^-] + [I_3^-]$) for the PMII/I_2 redox couple with constant molar ratios (PMII:I_2 = 10:1) in acetonitrile. (b) Calculated diffusion coefficient of I_3^- for both liquid and nanoclay gel.

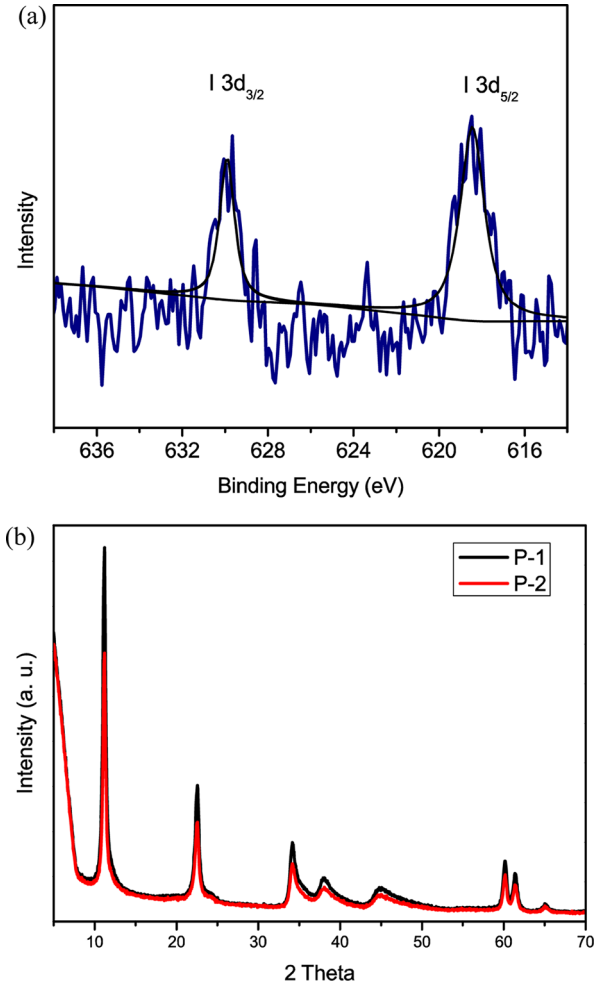

Figure 3. (a) X-ray photoelectron spectroscopic spectrum of I 3d in the nitrate-hydrotalcite clay powder extracted from gel electrolyte containing 1 M PMII and 0.1 M I_2. (b) Comparison of X-ray diffraction patterns of bare nitrate-hydrotalcite clay powder (pattern P-1, black trace) and the powder extracted from gel electrolyte (pattern P-2, red trace).

dx.doi.org/10.1021/am3025454 | ACS Appl. Mater. Interfaces 2013, 5, 444−450

existence of iodide contaminants in the nitrate-hydrotalcite clay powder is eliminated. The presence of iodide ions could be due to their exchange with the original nitrate ions. However, because of the similarity in size and ion affinity[45] between I_3^- and NO_3^- ions, no significant peak shift in the XRD spectrum is observed (see Figure 3b).

Shown clearly in Table 1, the nitrate-hydrotalcite nanoclay addition in liquid electrolyte enhances the V_{OC}. The theoretical V_{OC} value in DSC is determined by the potential difference between the Fermi energy of the TiO_2 electrode and the redox potential of triiodide/iodide in the electrolyte. The equilibrium potential of triiodide/iodide redox couples can be determined from the potential where the current become zero by ultramicroelectrode. According to steady-state voltammetric study (Figure 4), the redox potential remains unchanged after

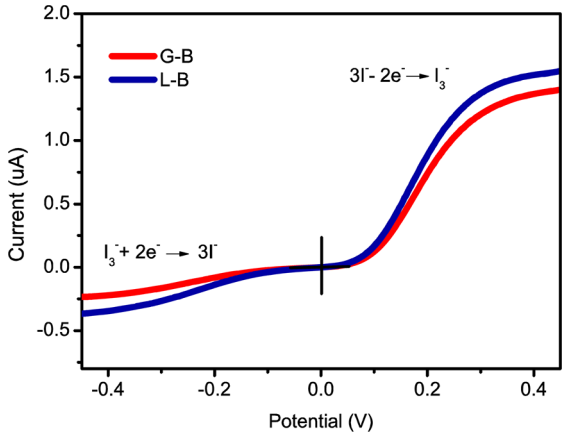

Figure 4. Cyclic voltammograms of AN-based liquid (L-B) and its nitrate-hydrotalcite clay gel electrolyte (10 wt % nanoclay content, labeled as G-B) with Pt microelectrode (scan rate = 10 mV/s).

the addition of nanoclay to the electrolyte. Consequently, the improvement of V_{OC} can only be attributed to the change in Fermi energy of TiO_2. The equilibrium Fermi energy of electrons in semiconductors can be expressed by the following equation:[46]

$$E_F = E_C + kT \ln\left(\frac{n_c}{N_c}\right) \quad (5)$$

where E_F is the Fermi energy, E_C the conduction band energy, kT the thermal energy, n_c is the electron concentration, and N_C the effective concentration of accessible electronic states in the conduction band.

The shift in the conduction band energy can be diagnosed from electrochemical impedance measurements of the chemical capacitance under light. Figure 5 shows the chemical capacitance versus open-circuit potential (V_{OC}) of TiO_2, based on different weight percentages of nanoclay in the electrolyte. At fixed capacitance, a continuous right shift of V_{OC} is observed with nanoclay content. Therefore, according to the equation described, the observed V_{OC} enhancement is attributed to the conduction band shift to a higher energy level after the addition of nitrate-hydrotalcite clay.

The change in V_{OC} with different weight percentages of nanoclay should be due to the basic nature of nitrate-hydrotalcite clay. Usually, the surface of TiO_2 can be more or less protonated, depending on the pH of the electrolyte.[47] Adding a base in the electrolyte deprotonates the surface of

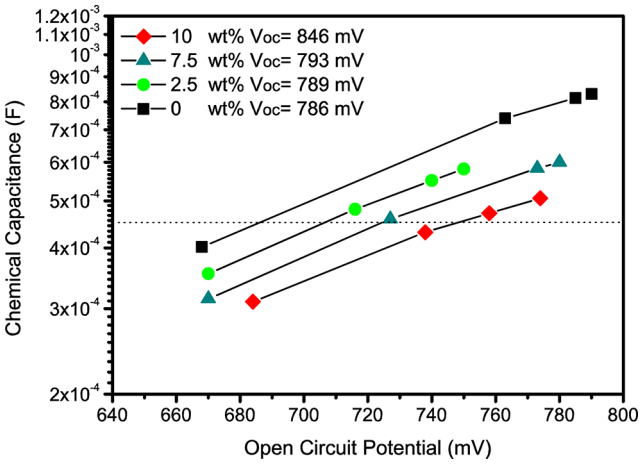

Figure 5. Chemical capacitance of TiO_2 photoanode extracted from electrochemical fitting of a semicircle obtained at an intermediate frequency region at different open-circuit potentials (V_{OC}). Different V_{OC} values are controlled by applying various intensity of LED light shining on devices (frequency range = 100 kHz−0.1 Hz, ac amplitude = 10 mV).

TiO_2 and results in an alternation of surface potential, which is the origin of band bending adjacent to the surface.[47−49] However, in DSCs, the nanoparticles used are too small to support a significant band bending.[47] As a consequence, the entire conduction band of the TiO_2 film shifts with the surface potential and, hence, results in an enhancement in V_{OC} for devices with nanoclay gel electrolytes. The phenomenon was also observed in a study of the effect of the addition of 4-*tert*-butylpyridine (TBP) in a liquid electrolyte, which has often been reported to act as a base in DSCs.[48]

Therefore, the origin of V_{OC} enhancement in nanoclay gel electrolyte can be attributed to a shift of the conduction band energy of TiO_2 to higher energy levels. This can be further verified using various dye systems with different LUMO levels. The obtained device performance with different dyes as a sensitizer using the nitrate-hydrotalcite nanoclay gel electrolyte is shown in Table 2. For organic dye D35, similar enhancement

Table 2. DSC Performance Comparison of Gel and Liquid Electrolyte with D35 and N749 Dyes

solar cell[a]	PCE (%)	J_{SC} (mA/cm^2)	V_{OC} (mV)	FF	ΔPCE[b] (%)
L-D35	5.9	11.9	712	0.70	
G-D35	6.5	11.7	769	0.72	10
L-N749	7.0	11.4	697	0.77	
G-N749	5.6	10.1	768	0.73	−20

[a]Data are obtained with photoanode 5 + 2 layers for D35, and 3 + 2 layers for N749. [b]$\Delta PCE = (PCE_G - PCE_L)/PCE_L$.

in the device performance is obtained mainly due to the V_{OC} enhancement and negligible change in J_{SC}. However, for ruthenium-based N749 dye, although an enhancement in V_{OC} was observed, the overall PCE decreased, because of the decrease in J_{SC}. According to the literature, the LUMO levels of D35, N719, and N749 dyes are at −1.37 eV,[50] −1.15 eV[51] and −0.77 eV,[52] respectively, vs NHE. The Fermi level of TiO_2 is between −0.4 eV and −0.5 eV.[53,54] The LUMO levels of D35 and N719 dyes are high enough and do not affect the electron injection, although there is an upward shift in conduction band of TiO_2 after the addition of nitrate-hydrotalcite nanoclay in the

dx.doi.org/10.1021/am3025454 | ACS Appl. Mater. Interfaces 2013, 5, 444−450

electrolyte. However, the LUMO level of the N749 dye is lower than that of the N719 dye. In this case, the additional effect of nitrate-hydrotalcite clay electrolyte on escalating the conduction band of TiO_2 could cause deficiency in electron injection, since there is a minimum energy difference of ~0.3 eV required for effective injection.[55]

Nitrate-hydrotalcite clay acts like a base, which can shift the conduction band of TiO_2 upward, and it is superior to basic salt additives, as shown in Table 3. The amount of NaOH added in the electrolyte is calculated by obtaining an equal pH value (pH 10) in water as 10 wt % of nanoclay added. Adding NaOH also enhances the V_{OC} but not as efficiently as nanoclay. However, the J_{SC} decreases significantly, compared to the pure liquid cell. The decrease in J_{SC} is not due to dye desorption by an alkaline source, because the amount of dye loaded on the photoanode is comparable after exposure to the electrolyte. However, while adding NaOH in the electrolyte, a small amount of aggregation of electrolyte species is observed. This degradation of the electrolyte with the presence of NaOH could be responsible for the decreased J_{SC} value. Unlike strong alkaline salts directly dissolving in the electrolyte, the nanoclay acts more like a buffering source, preventing the electrolyte from being too acidic, because of the presence of a large amount of iodide/iodine ions.

Table 3. Comparison of the Photovoltaic Characteristics of Liquid, Gel Electrolyte, and Liquid Electrolyte with the Addition of NaOH

solar cell[a]	PCE (%)	J_{SC} (mA/cm^2)	V_{OC} (mV)	FF	amount of dye[b] ($\times 10^{-8}$ mol)
L-NaOH	6.4	12.5	767	0.67	4.0
L-Nil	7.8	14.6	733	0.73	3.9
G-Nil	8.4	14.3	830	0.71	4.1

[a]L-NaOH, L-Nil, and G-Nil denote electrolyte conditions: liquid electrolyte with NaOH added, liquid electrolyte with no additional modification, and nanoclay gel with no additional modification. Data are obtained with photoanode 4 + 1 layers. [b]Measured in 0.1 M NaOH in water + ethanol (1:1 v:v).

CONCLUSIONS

We have achieved a 10% improvement in power conversion efficiency (PCE) for nitrate hydrotalcite nanoclay gel electrolyte solar cells (PCE = 9.6%) compared to their liquid electrolyte counterparts (PCE = 8.8%) under full sun illumination. In this clay gel system, charge transport is through physical diffusion, where the ions can diffuse smoothly through the channels developed by the clay networks. Thus, the calculated physical diffusion coefficient is not affected much by the viscosity of the gel electrolyte. The observed enhancement in open-circuit potential (V_{OC}) is due to the upward shift of the conduction band, which benefits from the buffering role of clay to prevent the electrolyte from being too acidic. The maximum PCE of 10.1% is achieved under 0.25 sun. This study demonstrates that nanoclay gel electrolyte improves PCE while alleviating critical problems for the liquid, such as solvent leakage.

EXPERIMENTAL SECTION

Materials and Methods. The Mg−Al hydrotalcite containing nitrate anions was prepared using the coprecipitation method[56] at constant pH; in brief, 0.011 mol $Al(NO_3)_3{\cdot}6H_2O$ (98+%, ACS reagent, Sigma−Aldrich) and 0.033 mol $Mg(NO_3)_2{\cdot}9H_2O$ (99%, ACS reagent, Sigma−Aldrich) were dissolved in 100 mL of deionized water (solution 1). Then, 0.15 mol NaOH (97+%, ACS reagent, pellets, Sigma−Aldrich) and 0.049 mol $NaNO_3$ (99+%, ACS reagent, Sigma−Aldrich) were dissolved in 50 mL of deionized water (solution 2). Solution 1 was added slowly into solution 2 with rapid stirring at 80 °C. The mixture was further stirred at 80 °C for 35−40 h and the precipitate obtained was subsequently washed with deionized water several times. The synthesized clay was ~50−80 nm in size and a few nanometers in thickness (see the SI).

The liquid electrolyte was composed of 1 M 1-propyl-3-methylimidazolium iodide (PMII), 0.1 M bis(trifluoromethane) sulfonimide lithium salt, 0.1 M iodine, and 0.5 M 1-methylbenzimidazole in commonly used AN or MPN solvent. The nanoclay gel electrolytes were prepared by dispersing different weight percentages of hydrotalcite nanoclay into the liquid electrolyte. The mixture was sonicated for 5−10 min at room temperature and subsequently homogenized using an ultrasonic homogenizer. Liquid electrolyte solidification (i.e., gel formation) occurs after more than 10 wt % of the nanoclay has been added (see the SI). As-prepared nanoclay gel electrolyte was subsequently used for device testing.

Transparent nanoporous TiO_2 photoanodes were prepared as follows: an FTO substrate was cleaned and treated with 40 mM $TiCl_4$ at 70 °C for 30 min. Subsequently, a nanocrystalline TiO_2 paste (18NRT Dyesol) was screen-printed on the substrate, followed by screen printing of a Ti-nanoxide paste (WER2-O, Dyesol), to act as scatter layers. Prepared films were then annealed on a hot plate at 325 °C for 5 min, 375 °C for 5 min, 450 °C for 15 min, 500 °C for 15 min, and then cooled to room temperature. Subsequently, cooled films were treated again with 40 mM $TiCl_4$ at 70 °C for 30 min and sintered at 500 °C for 30 min. After cooling, the TiO_2 films were immersed overnight in dye solution: 0.3 mM acetonitrile/*tert*-butyl alcohol (v:v = 1:1) solution of N719 dye ($[Ru(2,2'\text{-bipyridyl-}4,4'\text{-dicarboxylate})_2(NCS)_2]H_2(Bu_4N)_2$, Dyesol); 0.2 mM ethanol solution of organic dye coded D35; 0.3 mM N749 ($TBA_2[Ru(H_2tcterpy)(NCS)_3]$) in a mixture of acetonitrile and *tert*-butyl alcohol (v:v = 1:1).

Two holes were drilled 4 mm apart in the FTO substrates, for electrolyte filling. The hexachloroplatinic acid (8 mM in isopropanol solution) was drop-casted on the drilled conducting side of FTO glass and annealed at 400 °C for 15 min to reduce the Pt^{4+} ions. Prepared electrodes were used as counter electrodes for device fabrication. Fabrication of DSCs was done by sandwiching the dye-soaked TiO_2/FTO electrode and platinized FTO (counter electrode) with a 60-μm thermoplastic Suryln spacer (Surlyn, Solaronix) by hot pressing at 110 °C. The triiodide/iodide-based liquid electrolyte was introduced into sandwiched electrodes through the predrilled holes. Nanoclay-based gel electrolytes were shaken to form a liquid prior to injecting it into the cell through the holes of the counter electrode. Since the nanoclay gel electrolyte is thixotropic, its fluidity is increased by applying mechanical shear force.

Characterization. The surface morphology of the nanoclay was analyzed using field-emission scanning electron microscopy (FESEM; JEOL, Model JSM-7600F, 5 kV). The phase and crystallite size of the nanoclay were investigated by X-ray diffraction (XRD; Bruker Advance, Model AXS D8). X-ray photoelectron spectroscopy (XPS) analysis is performed using a Kratos-Axis spectrometer with monochromatic Al Kα (1486.71 eV) X-ray radiation (15 kV and 10 mA) and a hemispherical electron energy analyzer. The spectra are normalized according to C 1s at 284.5 eV.

The current−voltage (J−V) characteristics of the cells having an active area of 0.28 cm^2 or 0.16 cm^2 were measured under an illumination with AM 1.5 (100 mW/cm^2) using a solar simulator (San-EI Electric, Model XEC-301S) coupled with a digital source meter (Keithley) for recording the J−V plot. The data presented by the devices were averages from two cells. The steady-state voltammetry measurements for the liquid and a 10 wt % nanoclay gel electrolyte were carried out using an AutoLab Model PGSTAT302N system at a scan rate of 10 mV/s. A typical electrochemical cell equipped with a 10-μm-radius Pt microelectrode as a working electrode, and Pt foil and

Pt wire as the counter and quasi-reference electrodes, respectively, in liquid and nanoclay gel electrolyte.

The EIS characterization of the devices were carried out at open-circuit potential using a computer-controlled AutoLab PGSTAT302N system with a frequency range from 0.1 Hz to 100 kHz at a potential modulation of 10 mV. The obtained experimental data were fitted with the Z-view software (ZView 3.2b, Scribner Associates, Inc.), using appropriate equivalent circuits. The chemical capacitance was extracted from the fitting data.

■ ASSOCIATED CONTENT

Ⓢ Supporting Information

Supporting information includes the XPS spectrum of the reference clay, TEM images of nitrate-hydrotalcite nanoclay, and the picture of its gel electrolyte. This information is available free of charge via Internet at http://pubs.acs.org.

■ AUTHOR INFORMATION

Corresponding Author

*E-mails: subodh@ntu.edu.sg (S.G.M.), uchida@rcast.u-tokyo.ac.jp (S.U.).

Author Contributions

○These authors have equally contributed.

Notes

The authors declare no competing financial interest.

■ ACKNOWLEDGMENTS

The financial supports from Nanyang Technological University, Ministry of Education Singapore and Robert Bosch (sea) Pte Ltd, Energy Research Institute @ NTU are gratefully acknowledged. Funding from National Research Foundation (NRF) Singapore is also kindly acknowledged (CRP Award No. NRF-CRP4-2008-03). We deeply thank Dr. Lidong Sun, for his help in measurement of solar cell characteristics under different light intensities; Ms. Xiaoyan Wang, for XPS measurement; and Mr. Loc Huu Nguyen, for preparing the N749 cells.

■ REFERENCES

(1) O'Regan, B.; Gratzel, M. *Nature* **1991**, *353* (6346), 737−740.
(2) Gratzel, M. *Nature* **2001**, *414* (6861), 338−344.
(3) Muduli, S.; Lee, W.; Dhas, V.; Mujawar, S.; Dubey, M.; Vijayamohanan, K.; Han, S.-H.; Ogale, S. *ACS Appl. Mater. Interfaces* **2009**, *1* (9), 2030−2035.
(4) Meekins, B. H.; Kamat, P. V. *ACS Nano* **2009**, *3* (11), 3437−3446.
(5) Tai, Q.; Chen, B.; Guo, F.; Xu, S.; Hu, H.; Sebo, B.; Zhao, X.-Z. *ACS Nano* **2011**, *5* (5), 3795−3799.
(6) Kim, J. Y.; Noh, J. H.; Zhu, K.; Halverson, A. F.; Neale, N. R.; Park, S.; Hong, K. S.; Frank, A. J. *ACS Nano* **2011**, *5* (4), 2647−2656.
(7) Sun, L.; Zhang, S.; Wang, X.; Sun, X. W.; Ong, D. Y.; Kyaw, A. K. K. *Energy Environ. Sci.* **2011**, *4*, 2240−2248.
(8) Yella, A.; Lee, H.-W.; Tsao, H. N.; Yi, C.; Chandiran, A. K.; Nazeeruddin, M. K.; Diau, E. W.-G.; Yeh, C.-Y.; Zakeeruddin, S. M.; Grätzel, M. *Science* **2011**, *334* (6056), 629−634.
(9) Green, M. A.; Emery, K.; Hishikawa, Y.; Warta, W. *Prog. Photovolt. Res. Appl.* **2011**, *19* (1), 84−92.
(10) Michael, G. *J. Photochem. Photobiol., A* **2004**, *164* (1−3), 3−14.
(11) Bach, U.; Lupo, D.; Comte, P.; Moser, J. E.; Weissortel, F.; Salbeck, J.; Spreitzer, H.; Gratzel, M. *Nature* **1998**, *395* (6702), 583−585.
(12) Wang, P.; Zakeeruddin, S. M.; Moser, J. E.; Nazeeruddin, M. K.; Sekiguchi, T.; Gratzel, M. *Nat. Mater.* **2003**, *2* (6), 402−407.
(13) Wu, J. H.; Hao, S. C.; Lan, Z.; Lin, J. M.; Huang, M. L.; Huang, Y. F.; Fang, L. Q.; Yin, S.; Sato, T. *Adv. Funct. Mater.* **2007**, *17* (15), 2645−2652.
(14) Mulmudi, H. K.; Batabyal, S. K.; Rao, M.; Prabhakar, R. R.; Mathews, N.; Lam, Y. M.; Mhaisalkar, S. G. *Phys. Chem. Chem. Phys.* **2011**, *13*, 19307−19309.
(15) Leijtens, T.; Ding, I.-K.; Giovenzana, T.; Bloking, J. T.; McGehee, M. D.; Sellinger, A. *ACS Nano* **2012**, *6* (2), 1455−1462.
(16) Stathatos, E.; Lianos, P.; Lavrencic-Stangar, U.; Orel, B. *Adv. Mater.* **2002**, *14* (5), 354−357.
(17) Stergiopoulos, T.; Arabatzis, I. M.; Katsaros, G.; Falaras, P. *Nano Lett.* **2002**, *2* (11), 1259−1261.
(18) Gui, E. L.; Kang, A. M.; Pramana, S. S.; Yantara, N.; Mathews, N.; Mhaisalkar, S. G. *J. Electrochem. Soc.* **2012**, *159* (s3), B247−B250.
(19) Wu, J.; Lan, Z.; Hao, S.; Li, P.; Lin, J.; Huang, M.; Fang, L.; Huang, Y. *Pure Appl. Chem.* **2008**, *80* (11), 2241−2258.
(20) Katakabe, T.; Kawano, R.; Watanabe, M. *Electrochem. Solid-State Lett.* **2007**, *10* (6), F23−F25.
(21) Usui, H.; Matsui, H.; Tanabe, N.; Yanagida, S. *J. Photochem. Photobiol., A* **2004**, *164* (1−3), 97−101.
(22) Wang, P.; Zakeeruddin, S. M.; Comte, P.; Exnar, I.; Grätzel, M. *J. Am. Chem. Soc.* **2003**, *125* (5), 1166−1167.
(23) Jung, Y.; Son, Y.-H.; Lee, J.-K.; Phuoc, T. X.; Soong, Y.; Chyu, M. k. *ACS Appl. Mater. Interfaces* **2011**, *3* (9), 3515−3522.
(24) Lotsch, B. V.; Ozin, G. A. *ACS Nano* **2008**, *2* (10), 2065−2074.
(25) Tu, C.-W.; Liu, K.-Y.; Chien, A.-T.; Yen, M.-H.; Weng, T. H.; Ho, K.-C.; Lin, K.-F. *J. Polym. Sci., Part A: Polym. Chem.* **2008**, *46* (1), 47−53.
(26) Park, J. H.; Kim, B.-W.; Moon, J. H. *Electrochem. Solid-State Lett.* **2008**, *11* (10), B171−B173.
(27) Tsui, M.-C.; Tung, Y.-L.; Tsai, S.-Y.; Lan, C.-W. *J. Sol. Energy Eng.* **2011**, *133* (1), 011002.
(28) Inoue, T.; Uchida, S.; Kubo, T.; Segawa, H. Presented at the *2009 MRS Fall Meeting*, Paper No. R9.4, Boston, MA, Dec. 3, 2009
(29) Ghosh, P. K.; Bard, A. J. *J. Am. Chem. Soc.* **1983**, *105* (17), 5691−5693.
(30) Fitch, A. *Clays Clay Miner.* **1990**, *39* (4), 391−400.
(31) Misra, C.; Perrotta, A. J. *Clays Clay Miner.* **1992**, *40* (2), 145−150.
(32) Chen, C.-L.; Teng, H.; Lee, Y.-L. *Adv. Mater.* **2011**, *23* (36), 4199−4204.
(33) Nogueira, A. F.; Longo, C.; Paoli, M.-A. D. *Coord. Chem. Rev.* **2004**, *248*, 1455−1468.
(34) Kubo, W.; Kambe, S.; Nakade, S.; Kitamura, T.; Hanabusa, K.; Wada, Y.; Yanagida, S. *J. Phys. Chem. B* **2003**, *107* (18), 4374−4381.
(35) Kawano, R.; Watanabe, M. *Chem. Commun. (Cambridge, U.K.)* **2003**, *3*, 330−331.
(36) Rowley, J. G.; Farnum, B. H.; Ardo, S.; Meyer, G. J. *J. Phys. Chem. Lett.* **2010**, *1*, 3132−3140.
(37) Jeon, J.; Kim, H.; Goddard, W. A.; Pascal, T. A.; Lee, G.-I.; Kang, J. K. *J. Phys. Chem. Lett.* **2012**, *3*, 556−559.
(38) Kang, M.-S.; Ahn, K.-S.; Lee, J.-W. *J. Power Sources* **2008**, *180* (2), 896−901.
(39) Nazmutdinova, G.; Sensfuss, S.; Schrodner, M.; Hinsch, A.; Sastrawan, R.; Gerhard, D.; Himmler, S.; Wasserscheid, P. *Solid State Ionics* **2006**, *177* (35−36), 3141−3146.
(40) Ghosh, P. K.; Bard, A. J. *J. Am. Chem. Soc.* **1983**, *105*, 5691−5693.
(41) Ghosh, P. K.; Mau, A. W.-H.; Bard, A. J. *J. Electroanal. Chem. Interfacial Electrochem.* **1984**, *169*, 315−317.
(42) White, J. R.; Bard, A. J. *J. Electroanal. Chem. Interfacial Electrochem.* **1986**, *197*, 233−244.
(43) Furlani, C.; Mattogno, G.; Polzonetti, G.; Barbieri, R.; Rivarola, E.; Silvestri, A. *Inorg. Chim. Acta* **1981**, *52*, 23−28.
(44) Gaarenstroom, S. W.; Winograd, N. *J. Chem. Phys.* **1977**, *67* (8), 3500−3507.
(45) Miyata, S. *Clays Clay Miner.* **1983**, *31* (4), 305−311.
(46) Hagfeldt, A.; Boschloo, G.; Sun, L.; Kloo, L.; Pettersson, H. *Chem. Rev. (Washington, DC, U.S.)* **2010**, *110*, 6595−6663.

(47) Gratzel, M.; Durran, J. R. *Nanostructured and Photoelectrochemical Systems for Solar Photon Conversion*; World Scientific: Singapore, 2008.
(48) Boschloo, G.; Haggman, L.; Hagfeldt, A. *J. Phys. Chem. B* **2006**, *110*, 13144−13150.
(49) Mora-Sero, I.; Bisquert, J. *Nano Lett.* **2003**, *3* (7), 945−949.
(50) Hagberg, D. P.; Jiang, X.; Gabrielsson, E.; Linder, M.; Marinado, T.; Brinck, T.; Hagfeldt, A.; Sun, L. *J. Mater. Chem.* **2009**, *19*, 7232−7238.
(51) Matar, F.; Ghaddar, T. H.; Walley, K.; DosSantos, T.; Durrant, J. R.; O'Regan, B. *J. Mater. Chem.* **2008**, *18* (36), 4246−4253.
(52) Yang, S.-H.; Wu, K.-L.; Chi, Y.; Cheng, Y.-M.; Chou, P.-T. *Angew. Chem., Int. Ed. 50*, 8270−8274.
(53) Sun, Y.; Onicha, A. C.; Myahkostupov, M.; Castellano, F. N. *ACS Appl. Mater. Interfaces* **2010**, *2* (7), 2039−2045.
(54) Angelis, F. D.; Fantacci, S.; Mosconi, E.; Nazeeruddin, M. K.; Gratzel, M. *J. Phys. Chem. C* **2011**, *115*, 8825−8831.
(55) Marinado, T.; Hagberg, D. P.; Hedlund, M.; Edvinsson, T.; Johansson, E. M. J.; Boschloo, G.; Rensmo, H.; Brinck, T.; Sun, L.; Hagfeldt, A. *Phys. Chem. Chem. Phys.* **2009**, *11*, 133−141.
(56) Wegrzyn, A.; Rafalska-Lasocha, A.; Majda, D.; Dziembaj, R.; Papp, H. *J. Therm. Anal. Calorim.* **2010**, *99*, 443−457.